GEOPHYSICAL RESEARCH LETTERS, VOL. 36, L24304, doi:10.1029/2009GL040457, 2009

Northward thinning of Tibetan crust revealed by virtual seismic profiles

Tai-Lin Tseng,[1,2] Wang-Ping Chen,[1] and Robert L. Nowack[3]

Received 11 August 2009; revised 26 October 2009; accepted 20 November 2009; published 18 December 2009.

[1] A new approach of constructing deep-penetrating seismic profiles reveals significant, regional variations in crustal thickness under near-constant elevation of Tibet. Over distances of hundreds of kilometers, the crust is as thick as 75 km in southern Tibet but shoals to just over 60 km under the Qiangtang terrane in central Tibet where the deviation from Airy isostasy is equivalent to a thickness of over 10 km in missing crust. Northward thinning of crust occurs gradually over a distance of about 200 km where mechanical deformation, instead of pervasive magmatism, also seems to have disrupted the crust-mantle interface. **Citation:** Tseng, T.-L., W.-P. Chen, and R. L. Nowack (2009), Northward thinning of Tibetan crust revealed by virtual seismic profiles, *Geophys. Res. Lett.*, *36*, L24304, doi:10.1029/2009GL040457.

1. Introduction

[2] Tibet is the highest and largest plateau on the Earth. At least part of its high topography (~5 km above sea-level) is supported by buoyancy of a greatly thickened crust, or Airy isostasy [*Jimenez-Munt et al.*, 2008; *Owens and Zandt*, 1997]. However, it is the deviation from Airy isostasy that provides additional constraints on the dynamics of continental collision, such as effects of plate flexure [*Jiang et al.*, 2004; *Jin et al.*, 1996], convective instability [*Molnar et al.*, 1993], or deep-seated thermal buoyancy [*Jimenez-Munt et al.*, 2008; *Owens and Zandt*, 1997].

[3] In tectonically active regions, it is generally difficult to predict crustal thickness, or equivalently the depth to the Moho from topography. For instance, the actively extending Basin and Range province of western U.S. has high topographic relief but the Moho is remarkably flat in places where reliable data exist [e.g., *Klemperer et al.*, 1986]. For Tibet, using manmade sources near Lhasa, deep seismic reflection profiles in southern Tibet could not always detect the Moho [*Alsdorf et al.*, 1998; *Hauck et al.*, 1998]. Such negative results stood in contrast with that of *Hirn et al.* [1984], who used wide-angle seismic reflections generated by a small number of explosions and reported many large, abrupt offsets of the Moho, up to about 20 km in amplitude, despite low relief of the elevated surface. Discordant results regarding the Moho from deep seismic reflection and refraction have also been noted in many parts of the world [e.g., *Eaton*, 2006; *Hale and Thompson*, 1982; *Mooney et al.*, 1987], necessitating new approaches to constrain such a fundamental issue in geology.

[4] Using observations that were hundreds of kilometers apart, *Owens and Zandt* [1997] analyzed waveforms arising from conversions between compression- and shear-waves (*P*- and *S*-waves, respectively) across the Moho. Although the observations are too far apart to delineate regional characteristics, there seems to be a difference of about 10 km in crustal thickness between the Lhasa and the Qiangtang terranes in southern and central Tibet, respectively (see Figure 1b for locations of terranes). In contrast, over a distance of about 400 km in east-central Tibet where data from seismic arrays were available, recent studies using similar principles seemed to indicate smooth variations in crustal thickness across the two terranes [*Kind et al.*, 2002; *Shi et al.*, 2004].

[5] In this study, we use a novel approach to systematically investigate how thickened crust under Tibet varies over a large distance of about 550 km (Figure 1). The foundations of our work are the unprecedented resolution of dense-spaced, broadband seismic data from Project Hi-CLIMB [*Chen et al.*, 2007] and strong signal of reflections off the Moho from large earthquakes – a feature that cannot be replicated readily by manmade seismic sources. Interestingly, also using data from Hi-CLIMB, the latest results of seismic imaging showed a wide zone of disrupted Moho under central Tibet (R. Nowack et al., Application of Gaussian beam migration to multi-scale imaging of the lithosphere beneath the Hi-CLIMB array in Tibet, submitted to *Bulletin of the Seismological Society of America*, 2009), raising the question of how to evaluate the contribution from crustal isostasy to the overall support of Tibet's high elevation.

2. Virtual Seismic Profiles

[6] A direct, pragmatic approach is to determine average crustal properties from wide-angle reflections – prominent signals that, at periods longer than 5 s or so, are not particularly sensitive to fine details of the Moho interface (see Figure S3 and Text S1).[4] Figure 2 shows an example of how a clear seismic profile, comprised of consistently robust signals from the Moho (the seismic phase *SsPmp*), can be constructed over distances of hundreds of kilometers from a single earthquake source (Figure 1).

[7] *SsPmp* originates as the direct *S*-wave (*Ss* phase) reflects under the free surface and partially converts to *P*-wave, which, in turn, reflects off the top of the Moho

[1]Department of Geology, University of Illinois at Urbana-Champaign, Urbana, Illinois, USA.
[2]Now at Department of Geosciences, National Taiwan University, Taipei, Taiwan.
[3]Department of Earth and Atmospheric Sciences, Purdue University, West Lafayette, Indiana, USA.

0094-8276/09/2009GL040457$05.00

[4]Auxiliary materials are available in the HTML. doi:10.1029/2009GL040457.

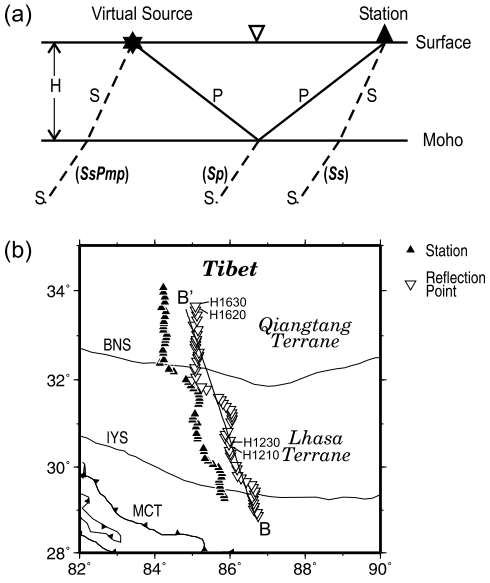

Figure 1. (a) A schematic diagram illustrating ray-paths of key crustal phases associated with a planar *S*-wave from a distant earthquake source. Notice that for *SsPmp*, the conversion from *S*- to *P*-waves under the free surface is a virtual source for subsequent *P*-reflection off the Moho. (b) A map showing the locations of Hi-CLIMB stations (solid triangles) used in this study and the corresponding points of reflections off the Moho associated with *SsPmp* (inverted triangles). The latter are calculated based on the location of the deep earthquake whose signals are used to construct the seismic profile along the solid line marked as BB′ (Figure 2). Thin, solid curves are key geologic boundaries on the surface: BNS, the Bangong-Nujian Suture; IYS, the Indus-Yarlong Suture; and MCT, the Main Central Thrust.

before finally arriving at a seismic station (Figure 1a). For the simple case of a crustal layer over a mantle half-space, the differential timing between *SsPmp* and *Ss* is

$$T_{SsPmp-Ss} = 2H\left(1/V_P^2 - p^2\right)^{1/2},$$

where p is the ray-parameter (horizontal slowness) of the incoming *S*-wave, H the crustal thickness, and V_P the average *P*-wave speed in the crust. In essence, the difference in travel-times between *SsPmp* and direct *S*-wave ($T_{SsPmp-Ss}$) is simply the two-way travel-time of obliquely reflected *P*-wave in the crust (Figure 1 and auxiliary material). Note that *SsPmp* undergoes total reflection (and a phase shift of $\pi/2$) at the bottom of the crust when p is greater than the reciprocal of the *P*-wave speed in the uppermost mantle.

[8] In Figure 2b, seismograms are aligned by direct *S*-wave pulses. For each seismogram, the corresponding arrival time of wide-angle *P*-reflection, or *SsPmp*, is marked by a triangular pointer in red. This type of seismic profile provides a powerful tool to probe the Moho even under greatly thickened crust. Notice that $T_{SsPmp-Ss}$ is as large as 14 s near the southern end of the profile and gradually changes northward to values around 12 s – direct evidence for varying average crustal thickness, H, and/or average *P*-wave speed in the crust, V_P, on a regional scale (Figure S2).

[9] Figure 2b is akin to a conventional seismic reflection profile in that although true illumination is from below, the point of *S*-to-*P* conversion under the free-surface is a virtual source for the subsequent reflection of *P*-wave off the top of the Moho [*Tseng and Chen*, 2006] (Figure 1a). As such, the *SsPmp* phase is equivalent to the prominent "*PmP*" phase in conventional seismic profiles [e.g., *Meissner et al.*, 2004]. Furthermore, for earthquake sources that are several thousand kilometers away, angles of incidence of the incoming *S*-wave are nearly constant across the entire profile (Table S1), so the geometry between each virtual source and its corresponding station remains essentially unchanged. Consequently the amplitude of *SsPmp* remains large at all stations, making it an easy task to precisely determine the relative timing between *SsPmp* and *Ss* across long profiles. The main difference between Figure 2b and traditional seismic reflection is that we trade near-vertical ray-paths for high amplitudes from wide-angle reflections.

[10] In the following analysis, we first set the mean V_P across the entire profile. This baseline value is about 6.3 km/s, consistent with previous studies in central and eastern Tibet [*Owens and Zandt*, 1997; *Zhao et al.*, 2001] (see auxiliary material and notice that the precise value of V_P is unimportant for detecting first-order, relative changes in crustal thickness among different stations.) We then calculate H from $T_{SsPmp-Ss}$ using laterally varying values of V_P reported by S.-H. Hung et al. (First multi-scale, finite-frequency tomography illuminates 3-D anatomy of the Tibetan plateau, submitted to *Geophysical Research Letters*, 2009). For the case at hand, even though $T_{SsPmp-Ss}$ depends on both H and V_P, detailed *P*-wave travel-time tomography showed that V_P varies by less than ±2% over the entire length of the profile [*Hung et al.*, 2008; also submitted manuscript, 2009]. Such fluctuations lead to small changes of about ±3 km in estimated crustal thickness, so observed differences in $T_{SsPmp-Ss}$ largely reflect changes in average crustal thickness (Figure 2b). Nevertheless, we allow a generous error of ±0.1 km/s in V_P when calculating the crustal thickness (error-bars in Figure 2c).

3. Deviation From Airy Isostasy and Implications

[11] The very thick crust under Tibet is by no means uniform; instead there is an overall trend of northward thinning (Figures 2b and 2c). Figure 3 compares average crustal thickness estimated from this study with detailed seismic imaging based on a rigorous treatment of scattered *S*-wavefield resulted from *P*-waves incident from below (Gaussian beam imaging of the phase *Ps* (Nowack et al., submitted manuscript, 2009)). As expected, near both ends of the profile where the Moho is sharp and smooth-varying, the two approaches give consistent results in crustal thickness. Notice that the Moho reaches its deepest depth, up to 73–77 km, beneath the southern Lhasa terrane (distances, x, between 0 and 200 km) but shoals to around 60–64 km beneath the Qiangtang terrrane (x between 420 and 550 km). Along these two segments of the profile, both the average thickness and V_P in the crust are tightly constrained by waveform modeling (discussed further in the auxiliary material); and it is evident that while the southern portion of the Lhasa terrane is close to Airy isostasy, deviation from crustal isostasy beneath the Qiangtang terrane is considerable, equivalent to a thickness of over 10 km in missing crust (Figure 2c).

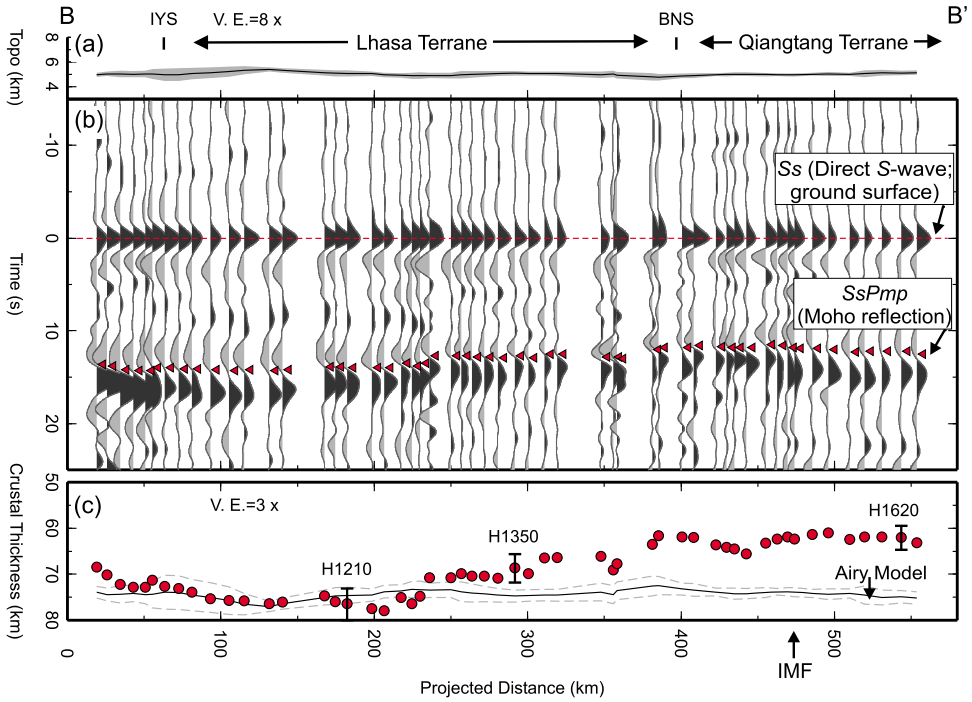

Figure 2. North–south trending profile across southern and central Tibet, showing topography, a *P*-wave reflection profile constructed using the seismic phase *SsPmp*, and estimated crustal thickness. (a) Mean elevation (solid curve) and its standard deviation (gray shading) across a swath of about 200 km in width, or the approximate separation between each virtual seismic source and station for *SsPmp*, along the profile. (b) A wide-angle, *P*-wave seismic profile constructed from *SsPmp* phases generated by an earthquake in 2005 (Table S1). The seismograms show broadband ground-velocity (vertical component data; zero-phase, Butterworth filter applied between 0.05 and 0.5 Hz). Due to total reflection off the top of the Moho, *SsPmp* has a phase-shift of $\pi/2$ when compared with the direct *S*-wave arrival (*Ss*). Note that the differential timing between *SsPmp* and *Ss* ($T_{SsPmp\text{-}Ss}$), a proxy for crustal thickness, decreases northward from ~14 s to ~12 s. (c) Estimated crustal thickness (red dots) based on $T_{SsPmp\text{-}Ss}$ and average *P*-wave speed in the crust (V_P), including perturbations to a background value of 6.30 km/s as determined from travel-time tomography (Hung et al., submitted manuscript, 2009). Vertical bars indicate generous estimate of errors in crustal thickness at representative stations ("H" followed by four-digit numerical codes). The solid curve shows predicted values from Airy isostasy (with the effect of one standard deviation from mean elevation marked by dashed curves.) IMF marks the horizontal position of the so-called Indian mantle front, or the leading (northern) edge of underthrust Indian mantle lithosphere [*Chen and Özalaybey*, 1998; Hung et al., submitted manuscript, 2009]. Other labels are BNS, the Bangong-Nujian Suture, and IYS, the Indus-Yarlong Suture.

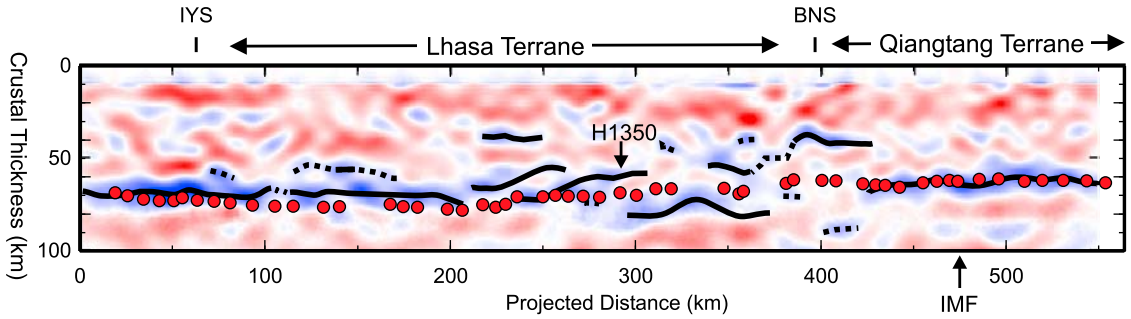

Figure 3. A comparison between crustal thickness estimated from wide-angle *P*-wave reflections (red dots; Figures 2b and 2c) and an image of the Tibetan lithosphere obtained by Gaussian beam migration of direct *P*- to *S*-wave conversions (Nowack et al., submitted manuscript, 2009). The convention is that a scatterer representing an increase in impedance with depth results in a blue pixel centered on the position of the scatterer. Black curves (dashed when uncertain), highlighting particularly strong impedance contrasts, show interpretations of the Moho transition zone by Nowack et al. (submitted manuscript, 2009). Notice near-constant crustal thickness over distances of hundreds of kilometers when the Moho is a simple interface near both ends of the profile. In the intervening zone of disrupted Moho, average crustal thickness decreases gradually northward by more than 10 km, from as much as 75 km to just over 60 km. Notice that the IMF is offset from the onset of shoaled Moho near the BNS. "H1350" marks the location of station whose observed waveform is discussed in detail (Figure S3).

[12] For illustrative purposes, the average density of crust is taken to be 2,800 kg/m^3, neglecting any lateral variations as corresponding changes in V_P are small [*Campbell and Heinz*, 1992; Hung et al., submitted manuscript, 2009]. The density increase across the Moho is assumed to be 450 kg/m^3 with a reference crustal thickness of 38 km at sea-level [*Jimenez-Munt et al.*, 2008]. Notice that isostatic supports below the Moho would have nearly identical effects on vertical positions of both the Moho and the free surface, so residual crustal thickness – the difference between observed and predicted values of crustal thickness from Airy isostasy (Figure 2c) – is a proxy for cumulative effects of isostasy in the mantle.

[13] Thinner crust under northern Tibet has been taken as evidence for full isostasy being achieved below the lithosphere, deep in the upper mantle where temperature is anomalously high [*Jimenez-Munt et al.*, 2008; *Owens and Zandt*, 1997]. Supporting evidence for such a mechanism includes inefficient propagation of head-waves just below the Moho [*McNamara et al.*, 1997; *Ni and Barazangi*, 1983], and large birefringence of *S*-waves [*McNamara et al.*, 1994] (up to 2 s or more between fast- and slow-directions of polarization) that has been inferred as a result of east–west flow in the upper mantle [*Owens and Zandt*, 1997]. Following this line of reasoning, the observation that thinner crust already starts appearing near the Bangong-Nujian suture (BNS, the surface join between Qiangtang and Lhasa terranes) implies that thermal isostasy in the mantle is at work immediately north of the Lhasa terrane.

[14] However, several independent pieces of evidences, including sudden drops of V_P and V_S in the upper mantle, abrupt increase in birefringence of *S*-waves, and modeling of gravity data indicate that the northern terminus of subhorizontally advancing Indian mantle lithosphere apparently continues for at least 70 km further north of the BNS (Figure 3) [e.g., *Chen and Özalaybey*, 1998; *Jin et al.*, 1996; Hung et al., submitted manuscript, 2009]. In other words, there is a distinct offset between where significant deviation from Airy isostasy begins and where thermal isostasy of the mantle becomes a plausible explanation. It is tempting to attribute this offset to flexure strength of either the Indian or the Tibetan mantle lithosphere, or perhaps the buoyancy of a chemically refractory Indian mantle lithosphere [*Jordan*, 1981]. At the moment, gravity data collected from Tibet remain proprietary, prohibiting further tests of this hypothesis.

[15] Intriguingly, the transition from an exceedingly large crustal thickness of over 70 km to values 10 km less than those expected from Airy isostasy largely coincides with the zone of highly disrupted Moho from Gaussian beam imaging (Figure 3), strongly suggesting that process(es) which disrupted the Moho also affected crustal thickness. In this zone, results summarized in Figure 2 delineate the position of a "seismic Moho" as detected by wide-angle reflection of *P*-waves. When the Moho is not a sharp interface, the seismic Moho is approximately at the midpoint of a gradual transition from crust to mantle. (A specific example, including results of waveform modeling, is presented in the auxiliary material.)

[16] This feature is qualitatively discernible in Figure 3 over much of the zone of disrupted Moho, between distances of about 250 to 420 km. Judging from results of multi-scale travel-time tomography based on finite-frequency theory, perturbations in V_P near the zone of disturbed Moho is small in both spatial extent and in amplitude (Hung et al., submitted manuscript, 2009). As such, empirical rules [*Birch*, 1961; *Campbell and Heinz*, 1992] relating V_P to crustal density ("Birch's law") would indicate that bulk composition of the crust has not been altered considerably; so disruption of Moho seems mainly a result of mechanical deformation, not major magmatic activities.

[17] In the zone of disrupted Moho, the position of the seismic Moho shows that average thickness of the crust gradually decreases northward; meanwhile, the deviation from Airy isostasy progressively increases (Figure 2c). Over scales of tens of kilometers, there is no obvious, abrupt steps in overall crustal thickness; and the deviation from crustal isostasy is about half of that at the far northern end of the profile (Figures 2b and 2c). Furthermore, a thinner crust under the northern Qiangtang terrane, by as much as 12 km when compared with the southern Lhasa terrane (Figure 2c), is consistent with earlier studies based on sparse observations along the Yadong-Golmud transect which lies almost 600 km to the east of our profile [*Mejia*, 2000; *Owens and Zandt*, 1997], suggesting that an overall northward thinning of Tibetan crust, or equivalently increasing deviation from Airy isostasy, may be a prominent, regional feature.

[18] **Acknowledgments.** The study was supported by U.S. National Science Foundation grants EAR99-09362 (Hi-CLIMB), EAR06-35419 and EAR06-35611 and U.S. Air Force contract FA8718-08-C-002.

References

Alsdorf, D. E., L. Brown, K. D. Nelson, Y. Makovsky, S. Klemperer, and W. Zhao (1998), Crustal deformation of the Lhasa terrane, Tibet plateau from project INDEPTH deep seismic reflection profiles, *Tectonics*, *17*(4), 501–519, doi:10.1029/98TC01315.

Birch, A. F. (1961), The velocity of compressional waves in rocks to 10 kilobars, part 2, *J. Geophys. Res.*, *66*(7), 2199–2224, doi:10.1029/JZ066i007p02199.

Campbell, A. J., and D. L. Heinz (1992), A high-pressure test of Birch's law, *Science*, *257*(5066), 66–68, doi:10.1126/science.257.5066.66.

Chen, W.-P., T.-L. Tseng, R. L. Nowack, S.-H. Hung, S.-L. Chung, and B.-S. Huang (2007), Mantle lithosphere beneath Tibet: A synthesis with special references to results from project Hi-CLIMB, *Eos Trans. AGU*, *88*(52), Fall Meet. Suppl., Abstract T23G-01.

Chen, W.-P., and S. Özalaybey (1998), Correlation between seismic anisotropy and Bouguer gravity anomalies in Tibet and its implications for lithospheric structures, *Geophys. J. Int.*, *135*(1), 93–101, doi:10.1046/j.1365-246X.1998.00611.x.

Eaton, D. W. (2006), Multi-genetic origin of the continental Moho: Insights from Lithoprobe, *Terra Nova*, *18*(1), 34–43, doi:10.1111/j.1365-3121.2005.00657.x.

Hale, L. D., and G. A. Thompson (1982), The seismic reflection character of the continental Mohorovicic discontinuity, *J. Geophys. Res.*, *87*(B6), 4625–4635, doi:10.1029/JB087iB06p04625.

Hauck, M. L., K. D. Nelson, L. D. Brown, W. Zhao, and A. R. Ross (1998), Crustal structure of the Himalayan orogen at ~90° east longitude from Project INDEPTH deep reflection profiles, *Tectonics*, *17*(4), 481–500, doi:10.1029/98TC01314.

Hirn, A., A. Nercessian, M. Sapin, G. Jobert, X. Z. Xin, G. E. Yuan, L. D. Yuan, and T. J. Wen (1984), Lhasa Block and bordering sutures: A continuation of a 500-km Moho traverse through Tibet, *Nature*, *307*(5946), 25–27, doi:10.1038/307025a0.

Hung, S.-H., W.-P. Chen, L.-Y. Chiao, T.-L. Tseng, and B.-S. Huang (2008), Three-dimensional seismic velocity structure of the crust and upper mantle beneath western Tibet from multiscale, finite-frequency travel-time tomography, *Eos Trans. AGU*, *89*(53), Fall Meet. Suppl., Abstract T11E-05.

Jiang, X., Y. Jin, and M. K. McNutt (2004), Lithospheric deformation beneath the Altyn Tagh and West Kunlun faults from recent gravity surveys, *J. Geophys. Res.*, *109*, B05406, doi:10.1029/2003JB002444.

Jimenez-Munt, I., M. Fernandez, J. Verges, and J. P. Platt (2008), Lithosphere structure underneath the Tibetan plateau inferred from elevation, gravity and geoid anomalies, *Earth Planet. Sci. Lett.*, *267*(1–2), 276–289, doi:10.1016/j.epsl.2007.11.045.

Jin, Y., M. K. McNutt, and Y. Zhu (1996), Mapping the descent of Indian and Eurasian plates beneath the Tibetan plateau from gravity anomalies, *J. Geophys. Res.*, *101*(B5), 11,275–11,290, doi:10.1029/96JB00531.

Jordan, T. H. (1981), Continents as a chemical boundary layer, *Philos. Trans. R. Soc. London*, *301*(1461), 359–373, doi:10.1098/rsta.1981.0117.

Kind, R., et al. (2002), Seismic images of crust and upper mantle beneath Tibet: Evidence for Eurasia plate subduction, *Science*, *298*, 1219–1221, doi:10.1126/science.1078115.

Klemperer, S. L., T. A. Hauge, E. C. Hauser, J. E. Oliver, and C. J. Potter (1986), The Moho in the northern Basin and Range Province, Nevada, along the COCORP 40°N seismic-reflection transect, *Geol. Soc. Am. Bull.*, *97*(5), 603–618, doi:10.1130/0016-7606(1986)97<603:TMITNB>2.0.CO;2.

McNamara, D. E., T. J. Owens, P. G. Silver, and F. T. Wu (1994), Shear wave anisotropy beneath the Tibetan plateau, *J. Geophys. Res.*, *99*(B7), 13,655–13,665, doi:10.1029/93JB03406.

McNamara, D. E., T. J. Owens, W. R. Walter, and C. J. Ammon (1997), Upper mantle velocity structure beneath the Tibetan plateau from *Pn* travel time tomography, *J. Geophys. Res.*, *102*, 493–505, doi:10.1029/96JB02112.

Meissner, R., F. Tilmann, and S. Haines (2004), About the lithospheric structure of central Tibet, based on seismic data from the INDEPTH III profile, *Tectonophysics*, *380*(1–2), 1–25, doi:10.1016/j.tecto.2003.11.007.

Mejia, J. A. (2000), Lithospheric structure beneath the Tibetan plateau using simultaneous inversion of surface wave dispersion and receiver functions, Ph. D. thesis, Saint Louis Univ., Saint Louis, Mo.

Molnar, P., P. England, and J. Martinod (1993), Mantle dynamics, uplift of the Tibetan plateau, and the Indian monsoon, *Rev. Geophys.*, *31*, 357–396, doi:10.1029/93RG02030.

Mooney, W. D., T. M. Brocher, D. Matthews, and C. Smith (1987), Coincident seismic reflection/refraction studies of the continental lithosphere: A global review, *Geophys. J. R. Astron. Soc.*, *89*(1), 1–6.

Ni, J., and M. Barazangi (1983), High-frequency seismic wave propagation beneath the Indian Shield, Himalayan Arc, Tibetan plateau and surrounding regions: High uppermost mantle velocities and efficient *Sn* propagation beneath Tibet, *Geophys. J. R. Astron. Soc.*, *72*(3), 665–689.

Owens, T. J., and G. Zandt (1997), Implications of crustal property variations for models of Tibetan plateau evolution, *Nature*, *387*(6628), 37–43, doi:10.1038/387037a0.

Shi, D., et al. (2004), Detection of southward intracontinental subduction of Tibetan lithosphere along the Bangong-Nujiang suture by *P*-to-*S* converted waves, *Geology*, *32*(3), 209–212, doi:10.1130/G19814.1.

Tseng, T.-L., and W.-P. Chen (2006), Probing the southern Indian shield with *P*-wave receiver-function profiles, *Bull. Seismol. Soc. Am.*, *96*(1), 328–333, doi:10.1785/0120050074.

Zhao, W., et al. (2001), Crustal structure of central Tibet as derived from project INDEPTH wide-angle seismic data, *Geophys. J. Int.*, *145*, 486–498, doi:10.1046/j.0956-540x.2001.01402.x.

W.-P. Chen, Department of Geology, University of Illinois at Urbana-Champaign, Urbana, IL 61801-2939, USA.

R. L. Nowack, Department of Earth and Atmospheric Sciences, Purdue University, West Lafayette, IN 47907, USA.

T.-L. Tseng, Department of Geosciences, National Taiwan University, Taipei 106, Taiwan. (tailintseng@ntu.edu.tw)